Microchemical Journal 204 (2024) 111121

Contents lists available at ScienceDirect

Microchemical Journal

journal homepage: www.elsevier.com/locate/microc

A high performance differential sensing system based on molecularly imprinted polymer for specific propofol concentration monitoring

Bowen Yang [a], Li Jin [a], Ze Xu [a], Wenwen Wang [a], Guanjun Wang [b], Jizhou Wu [a,c], Dandan Sun [a,*], Jie Ma [a,c]

[a] School of Physics and Electronic Engineering, Shanxi University, Taiyuan 030006, China
[b] School of Information and Communication Engineering, Hainan University, Haikou 570228, China
[c] Collaborative Innovation Center of Extreme Optics, Shanxi University, Taiyuan 030006, China

ARTICLE INFO

Keywords:
Propofol
Molecularly imprinted polymer
Microfiber interferometer
Fiber Bragg Grating
Differential demodulation

ABSTRACT

In this paper, a high performance differential sensing system combining microfiber interferometer (MFI) and fiber Bragg gratings (FBGs) based on molecularly imprinted polymer (MIP) film is proposed for specific propofol concentration detection. Surface refractive index changes are translated into interference wavelength shift resulting in the change of grating power difference, which helps simplify demodulation equipment. Beta-cyclodextrin (β-CD) assisted MIP film enables optic-fiber system to have specific recognition of propofol. Experimental results show that the sensing system has an obvious response to propofol in the concentration range of 0.001–10 mM, and a sensitivity of 6.04 nm/mM and the optimal sensitivity of differential modulation is 10.89 dB/mM in the concentration range of 0.001–0.05 mM. The sensing system also has excellent stability and specificity in artificial urine environment. The proposed sensing system not only provides a new method for the determination of propofol concentration, broadens the application field of optical sensor, and provides a new platform for application in biomedicine fields.

1. Introduction

Continuous total intravenous infusion of propofol is widely used in surgery as an important method to maintain general anesthesia [1]. After intravenous administration of propofol, there is a rapid balance between plasma and highly perfused brain tissue, which is the reason for the rapid onset of anesthesia. Furthermore, propofol can decompose in a short period of time, thus the abuse of propofol is particularly easily masked, which generates potential tolerance, psychological dependence, and even death [2]. The concentration of anesthesia must be immediately distinguished for diagnosis, and there is currently no method to measure or detect the concentration of anesthetic propofol in real time. Therefore, it is necessary to establish a highly sensitive and simple sensing system for the real-time monitoring propofol concentration.

In previous studies, there are three main methods for detecting propofol concentration. The first method is chromatography, which can be used for detection in high-performance liquid chromatography (HPLC) and gas chromatography-mass spectrometry (GC-MS). Jason Yarbrough et al. have established and validated the HPLC method for determining the content of propofol [3]. Wakako Hikiji, et al. have used a selective ion monitoring mode for determining propofol in human whole blood, brain, liver, and adipose tissue using the GC-MS method [4]. Chromatography can be used in combination with various measurement techniques, however, this approach is not capable of continuous monitoring and necessitates large and costly equipment. The second method is to use electrochemical technology to detect propofol. David C. Ferrier et al. have used an enzyme based electrochemical biosensor based on cytochrome P450 2B6, gold nanoparticles, and chitosan membrane to detect propofol [5]. Chandan Kafey et al. have designed an electrochemical microchannel sensor based on $Ti_3C_2T_x$ reduced graphene oxide (rGO) chitosan microchannels for detecting propofol solution [6]. However, the passivation of the electrode surface may occur from the formation of insoluble polymers on the electrode caused by the electrochemical oxidation of propofol. The third method is to detect propofol through optical method. Chien-Chong Hong et al. have proposed a handheld analyzer with disposable lab-on-a-chip technology for the electrical detection of the anesthetic propofol in

* Corresponding author.
E-mail address: sundd@sxu.edu.cn (D. Sun).

https://doi.org/10.1016/j.microc.2024.111121
Received 15 April 2024; Received in revised form 9 June 2024; Accepted 1 July 2024
Available online 2 July 2024

human plasma samples for clinical diagnoses [1]. Francisco U. Hernandez et al. have prepared a U-shaped functional fiber optic sensor for detecting propofol concentration using molecularly imprinted polymers (MIP) liquid phase deposition protocol technology [7]. The optical method is expected to make up for the defects of the other methods, and realizes a highly sensitive, simple and rust-proof biochemical detection technology. As a promising approach, molecular imprinting technology (MIT) possess the major unique features of structure predictability, recognition specificity and application universality, which has received widespread attention and become attractive in many fields.

The combination of MIT and fiber optic sensors has many applications in substance specific detection. Anand M. Shrivastav, et al. have reported the preparation and characterization of a surface plasmon resonance based fiber optic sensor for molecular imprinting detection of melamine within the range of melamine concentration from 10^{-7}M to 10^{-1}M [8]. Harshit Agrawal, et al. have designed a successful preparation and characterization of a MIP surface plasmon resonance based fiber optic sensor for detecting atrazine with the detection concentration range of 0 M to 10^{-7}M [9]. Pintu Gorai et al. have designed optical sensor that utilizes a combination of photonic crystal fiber based mode interferometry and MIP nanoparticles to exhibit specific and reproducible detection performance in the detection range of 10^{-8} to 10^{-3}M [10]. The above research progress can be seen that fiber optic sensor provide a number of benefits, including low cost, corrosion resistance, high sensitivity, resistance to electromagnetic interference, and compact size and light weight. Combining molecular imprinting, this sensor has significant advantages in improving the specificity of detecting target molecule.

In this study, a MIP differential sensing system combining microfiber interferometer (MFI) and fiber Bragg gratings (FBGs) is proposed and verified for the specific detection of propofol concentration. Surface refractive index changes are translated into interference wavelength shift resulting in the change of grating power difference, which help simplify demodulation method. The detected RI sensitivity responses are 1294.46 nm/RIU (MFI) and 2957.26 dB/RIU (FBGs), and the corresponding low temperature responses are − 0.07 nm/℃ (MFI) and 0.35 dB/℃ (FBGs). Subsequent experimental analysis have showed that the detected significantly propofol is in the concentration range of 0.001–10 mM, with sensitivity of 6.04 nm/mM and 10.89 dB/mM, and the system also has excellent sensing performance in artificial urine environment. This system presents a new compact all-fiber inquiry scheme, which has stability and specificity, and can serve as a platform for various biochemical detection.

2. Materials and methods

2.1. Reagents and instruments

Dopamine hydrochloride (98 %), Tris-Hydrochloride (pH8.5), 2,6–Diisopropylphenol (98 %), β-CD (98 %), and Triton x–100 (biotech grade) are purchased from Shanghai Macklin Biochemical Co., Ltd. (Shanghai, China). In the course of the experiment, deionised water (DIconductivity is 200–10 μs/cm) was used. The sample membrane was characterised by Fourier transform infrared spectrometer (FTIR ATR, Burker ALPHAII, Germany), and the surface of microfiber was characterised by scanning electron microscope (SEM, Teslacan Mira4 HITACHI Regulus8100, Japan; Zeiss Sigma 300, Germany).

In this paper, we used the photosensitive single-mode fiber (Nufern, USA, GF3). The reason for using this fiber is that its high contrast and high sensitivity to refractive index make it easier to make microfiber interferometer for better sensing performance. Amplified spontaneous emission light source (ASE, Minchuang Optoelectronics, China, range of 1528–1603 nm, power of 10dBm), and spectral analyser (OSA, Anritsu, Japan, AnritsuMS9740A, range of 600–1750 nm). Equipment used in the preparation of MFI had optical fiber welding machine (Fujikura FSM-60S, Japan) and motion controller (Zolix, MC600, China). In addition, digital refractive index metre (Reichert 13940000, United States) was used to measure the refractive index of the solution, optical photopower metre (OPM, LT500DB, China) was used to measure the intensity change in the optical path, and metallurgical microscope (Caikon, DMM–200C, China) was used to observe the macrostructure of optical. The groove moulds used in the experiment was made using a 3D printer (DDKUN, D160max, China).

2.2. Experimental setup

All fiber differential sensing system was shown in Fig. 1. The optical signal was sent from the ASE light source with an output power of 10 dB, transmitted to the MFI, through the circulator$_1$ to the FBG$_1$, then to the FBG$_2$, followed by the circulator$_2$, and finally collected by the OSA with a resolution of 0.03 nm to record the interference spectrum at this moment. In addition, circulator has three interfaces, Part 1, 2, and 3. The optical signal enters the circulator from Part 1, leaves from Part 2, and enters the next optical device. Part 3 is used to connect OPM, the OPM$_1$, OPM$_2$ can detect the intensity of the FBG$_{1,2}$ to simplify the demodulation equipment. In Section 1 of the Supplementary Material, Table S1 and S2 discussed the preparation process of FBGs and the specific parameters.

2.3. The microfiber interferometer fabrication

The MFI adopted a single-mode fiber-germanium-doped fiber-single-mode fiber combination structure. We used a butane flame to heat the germanium-doped fiber for 5–10 s. Then, the diameter of the optical fiber was gradually narrowed from 125 μm to about micron-meter scale, and a kind of MFI with high sensitivity and good stability was prepared. In order to minimize the experimental error, we had set the parameters of the motion controller including the motion distance of 18 mm, the speed of 2 mm/s, the acceleration of 5 mm/s^2, and the maximum speed of 9 mm/s. The part circled by the red dotted line in Fig. 1 showed the structure parameters of the MFI were annotated. These paremeters included two transition regions of 3 mm and a waist region of 13 mm length and approximately 10 μm diameter. In Section 2 of the Supplementary Material, Fig. S1 and Table S3 discussed the RI sensitivity of MFIs with different structural parameters. The blue arrow above was the macroscopic structure of the various parts of the MFI, which was the actual pattern observed by the metallurgical microscope. The reason for using germanium-doped fiber is that its high contrast and high sensitivity to refractive index make it easier to make MFI and have better sensing performance [11–13]. Compared with ordinary fiber, germanium-doped fiber has higher core refractive index and lower optical loss [14,15]. The Coating Material for germanium-doped fiber is Acrylate.

3. Results and discussion

3.1. Sensor principle

3.1.1. Principle of microfiber interferometer

Tapered optical fiber requires two taper sections used as optical components to construct the MFI diverse applications. The core and cladding modes are transmitted simultaneously with the mainly propagating fundamental mode (HE$_{11}$) and higher-order mode (HE$_{12}$) [16]. These tapered joints in optical fiber are used to couple the large amount of light energy of fundamental mode to the cladding modes. When the light passes through the first tapered part, the energy field distribution of the fundamental mode cannot change rapidly due to the small diameter, so that the local fundamental mode remains in the tapered region. This will result in leakage of the evanescent wave through the cladding area. Thus, the energy loss of the fundamental mode is converted to the higher-order cladding mode.This phenomenon is known as the core-cladding transition [17]. At the steep slope of the taper region, a large number of modes are excited and coupled with the guided light into high-order modes. These higher-order modes are coupled back to

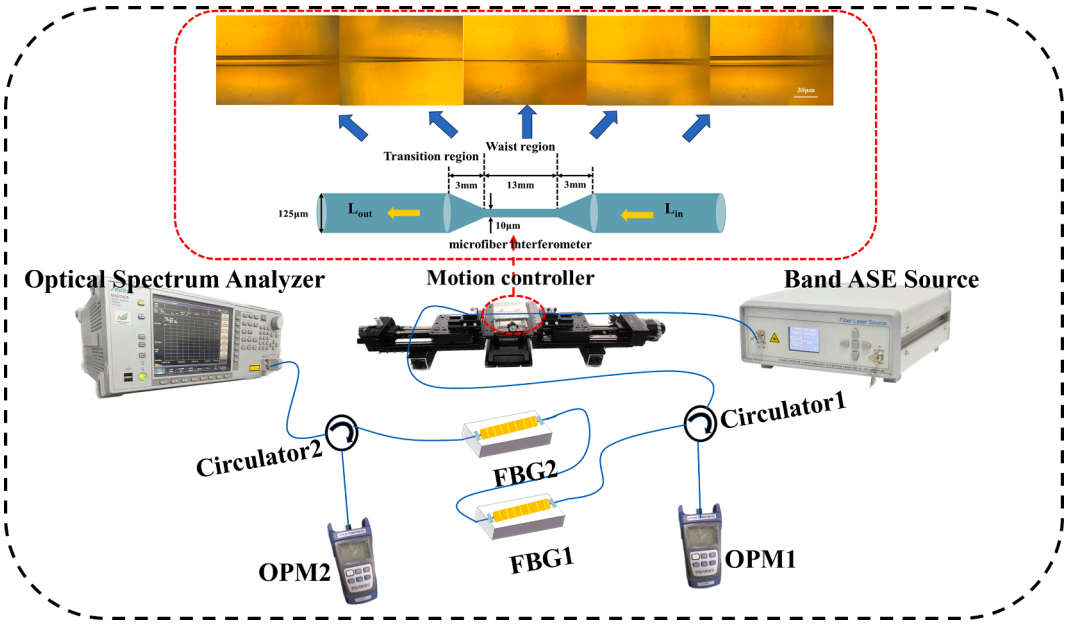

Fig. 1. Composition of high sensitivity differential sensing system. The part of the red dotted line are the MFI and the real picture of each part of the MFI observed by a metallurgical microscope.

the fundamental mode in the second taper region for producing interference, as shown in Fig. 2 (a).

The peak wavelength of Mach-Zehnder interferometer (MZI) spectrum can be calculated by the following formula [18]:

$$\lambda_m = \Delta n_{eff} L/m, (m = 1, 2, 3, ...) \quad (1)$$

where m is the order of MZI interference fringes, L is the length of MZI, Δn_{eff} is the effective refractive index (RI) difference between the cladding and the core.

Thus, the free spectral range (FSR) of MZI is as follows:

$$FSR = \lambda^2/\Delta n_{eff} L \quad (2)$$

In general, the external sensitivity RI of an interferometer can be expressed as [19]:

$$d\lambda/dn_{ext} = \lambda \bullet 1/\Gamma \bullet \left(1/\Delta n_{eff} \bullet d\Delta n_{eff}/dn_{ext}\right) \quad (3)$$

Among them, $\Gamma = 1 - \lambda/\Delta n \bullet d\Delta n/d\lambda$ is dispersion coefficient, which shows that the exponential difference is affected by the wavelength and RI change. And $d\Delta n_{eff}/dn_{ext}$ is the index dependent change caused by small changes in RI of the external environment. When the external RI increases, the effective exponents of both fundamental and higher-order modes rise correspondingly [20]. It is the exponential difference due to the tiny diameter of the microfiber that leads to its high RI sensitivity.

Therefore, when the functional film is attached to the surface of the microfiber, it constitutes a microfiber sensing probe to detect a specific substance. When the probe detects different concentrations of propofol, the wavelength shifts due to the RI surface changes.

3.1.2. Principle of fiber Bragg grating

FBG is a periodic perturbation of refractive index along optical fiber core. The formula for the reflected wavelength can be expressed as [21]:

$$\lambda_B = 2n_{eff}\Lambda \quad (4)$$

where λ_B is the central wavelength of FBG, n_{eff} is the effective refractive index of the optical fiber core, and Λ is the grating period.

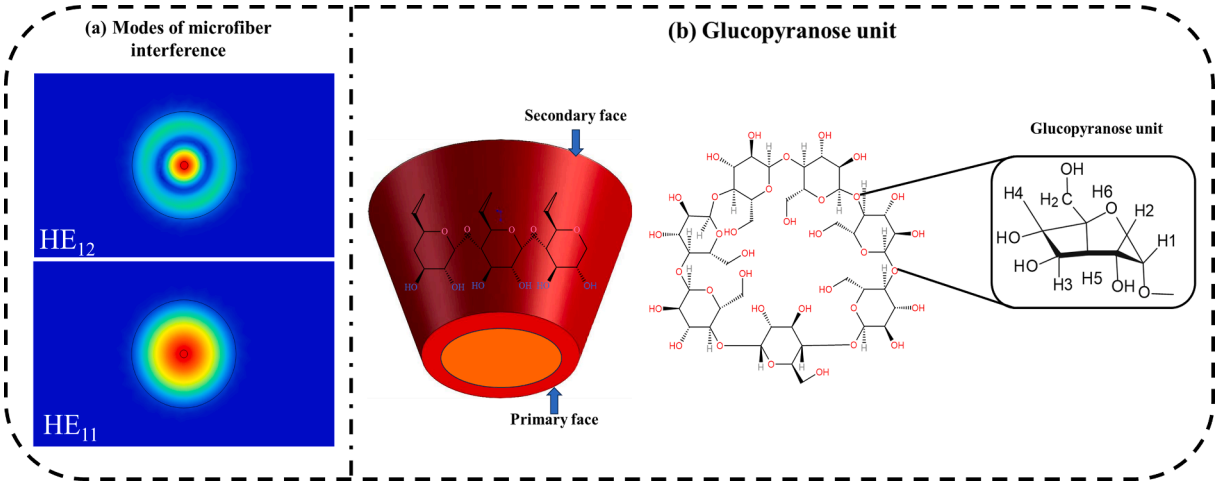

Fig. 2. (a) The transverse electric field amplitude distribution of HE_{11} and HE_{12} in the main interference mode. (b) β-CD (hosts) and propofol molecule (guest) can form inclusion complexes through host–guest interactions.

Two FBGs are selected so that they fall on the rising and falling edges of the two adjacent peaks of the interference spectrum. As the surrounding refractive index (SRI) increases, the RI difference between the core and cladding is reduced, then the effective RI of the MFI increases because of the Goos-Hänchen shift [22], Therefore, the peak wavelength of the MZI will shift to the longer wavelength while the Bragg wavelength keeps unchanged. In addition, the two slopes of the transmission spectrum of the MFI are opposite, thus the reflection intensities of the two FBGs change in the opposite trend. Their intensity difference is more sensitive to the SRI than any of the single reflective intensity of two FBGs, which can be written as:

$$\begin{aligned}\Delta I &= I_1 - I_2 \\ &= \int_{-\infty}^{+\infty} S(\lambda) \bullet T_1(\lambda - \Delta\lambda) \bullet R_1 \bullet \delta(\lambda - \lambda_1) d\lambda - \int_{-\infty}^{+\infty} S(\lambda) \bullet T_2(\lambda - \Delta\lambda) \\ &\quad \bullet R_2 \bullet \delta(\lambda - \lambda_2) d\lambda \\ &= R_1 S(\lambda_1) T_1(\lambda_1 - \Delta\lambda) - R_2 S(\lambda_2) T_2(\lambda_2 - \Delta\lambda)\end{aligned} \tag{5}$$

where ΔI is the differential intensity of the two FBGs, I_1 and I_2 are the reflective intensities of the FBG_1 and FBG_2. $S(\lambda)$ is the power spectral density function of light source, $T_1(\lambda)$ and $T_2(\lambda)$ are the initial transmission spectrum functions of the two linear regions of the MFI. λ_1 and λ_2 are the Bragg wavelengths of FBG_1 and FBG_2. $\Delta\lambda$ is the wavelength shift of the spectrum of the MFI induced by the change of the SRI. R_1 and R_2 are the reflective coefficients of the FBG_1 and FBG_2. $\delta()$ is the unit impulse function. $R_1\delta(\lambda - \lambda_1)$ and $R_2\delta(\lambda - \lambda_2)$ are the reflective spectrum functions of the FBGs which are described as impulse functions because the bandwidths of the FBGs are far smaller than that of the MFI. Thus, the SRI measurement can be accomplished by calculating the differential intensity of the two FBGs. Besides, the MFI is blue shift, which results in the advantage of minimal temperature dependence for the RI measurement. Because their response to temperature is relatively small, the grating wavelength difference between the two FBGs can help the refractive index measurement to eliminate cross-sensitivity.

3.1.3. Synthesis of propofol imprinted polymer

The approach used in this study detects capture of propofol on the surface of the MFI with the aid of cyclodextrins. Cyclodextrins Fig. 2. (b) are offer an alternative for its biocompatibility and have been used as a host compounds for other type of analytes [23,24].

The MIT used in this sensor is to recognize propofol specifically through the host-guest interaction between the propofol binding sites assisted by cyclodextrin and embedded in the PDA film formed on the fiber surface.Through the host-guest interaction between the propofol binding sites assisted by cyclodextrin, it is embedded in the PDA film formed on the fiber surface for specific recognition of propofol. This step of the process is that the functional groups are kept in place by a highly cross-linked polymer matrix, thus trapping the template in a rigid cavity. Consequently, the pre-polymerization complex is formed. Finally, the template is removed from the resulting polymer matrix to obtain MIP.

The application of MIT in this sensor is achieved by the following specific film preparation, as shown in Fig. 3.The formation process of PDA is shown in Step 1 of Fig. 3. Dopamine (DA) is oxidized to 5,6–dihydroxyindole (DHI) under alkaline conditions (Tris-Hydrochloride, pH = 8.5), and further polymerized to polydopamine [25]. The most relevant reasons for the super-adhesive properties of PDA are the presence of catechol functional groups that can form covalent or non-covalent bonds (hydrogen bonds, van der Waalsforces, or stacking forces) with the surface of the substrate material [26]. Therefore, β-CD can also be attached to PDA, and the combination of both can be attached to the specific microfiber biological probe.The next part of Step 1 in Fig. 3 is the 3D model of the three substances, where the positions of hydrogen bonds and covalent bonds can be clearly seen.

According to the polymer formation principle described above, β-CD: propofol (v: v 1: 1) mixed solution is on the coated PDA microfiber. As mentioned above, the PDA has strong bonding properties, so the polymer can adhere to the surface of the PDA, as shown in Fig. 3. Step 2.

As shown in Fig. 3 Step 3, in order to enable the film to have specific recognition of propofol, a template removal solution (Tratone x–100: DI water v: v 1: 10) is used to eluate the propofol on the surface of the film, and the MIP film for the detection of propofol is established.

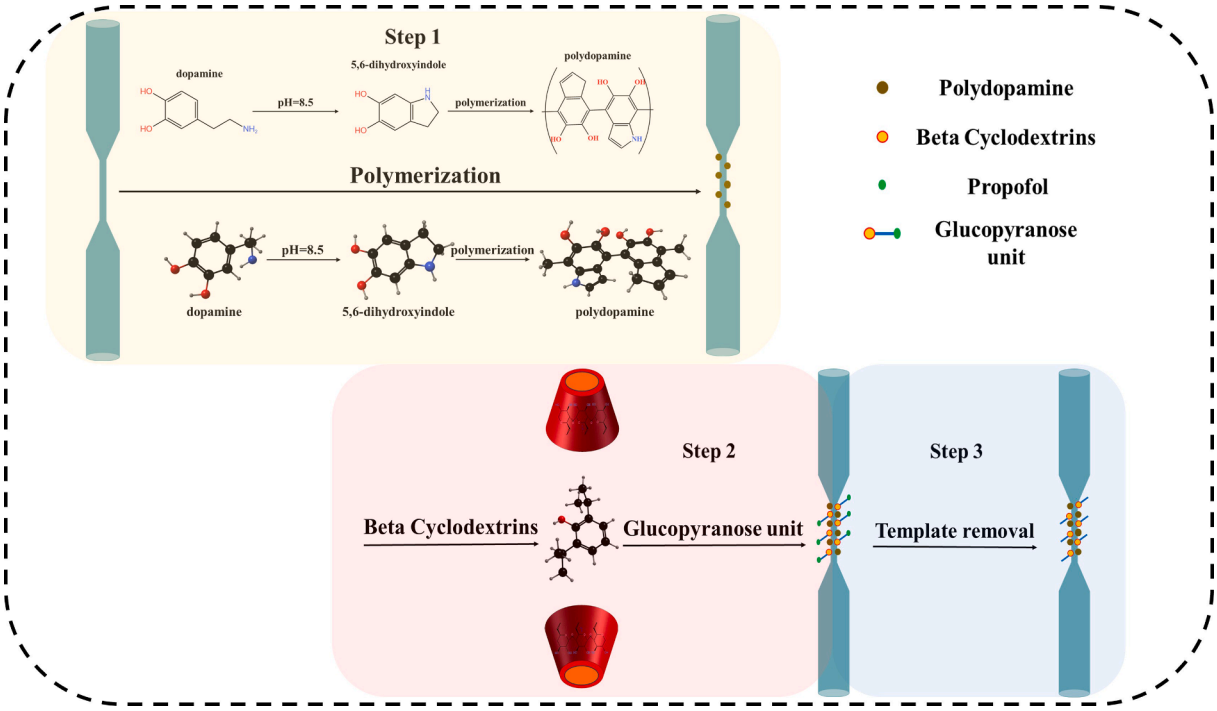

Fig. 3. The principle and preparation of MIP optic fiber sensor.

3.2. Refractive index and temperature performance

Fig. 4 (a, top) shows the original spectrum of the MFI and two FBGs combined differential sensing system, in which the part marked with black letters are the position of FBGs on the interference spectrum. In order to accurately measure the sensing performance of the differential sensing system to the change of external RI, the sodium chloride solution is used to simulate the external RI solution, and the digital refractometer is used to detect the RI value of the sodium chloride solution. Fig. 4 (a, bottom) shows the redshift spectrums of different RI solutions are recorded at room temperature (26℃). Fig. 4 (b, top) shows that the power changes of two FBGs with the increase of RI value. It can be seen that with the gradual increase of RI value, the power of FBG_1 gradually increases and the power of FBG_2 gradually decreases. The two FBGs are used to make a difference to improve the estimation accuracy of the total spectral frequency shift. When the output spectrum experienced a red-shift, the intensity of the FBG peaks changed accordingly [27]. It can be seen in Fig. 4 (b, bottom) that the RI sensitivity of the MFI and $FBG_1 - FBG_2$ power difference are 1294.46 nm/RIU and 2957.26 dB/RIU in the range of 1.3387 to 1.3415, respectively. Based on the following formula (6) [20], their LOD for refractive index are 0.00003 RIU (MFI) and 0.000009 RIU (FBG), respectively.

$$LOD = 3\delta/S \tag{6}$$

In addition, the temperature analysis is performed for the range from 30 to 70℃. The MFI and FBGs are placed simultaneously in a thermostat and the spectrums are recorded every 5℃. In order to ensure the uniform heating to minimize experimental error, it is very important that before storing the spectral data, the temperature needs to keep 5 min for reaching the preset value. In Fig. 4 (c,top), the wavelength of the FBGs transmission spectrum tends to red-shift as the ambient temperature increases, and the linear fit shows a low temperature sensitivity of FBG_1 of 0.008 nm/℃ and FBG_2 of 0.009 nm/℃. It can be seen in Fig. 4 (c, bottom) that the temperature sensitivity of the MFI and $FBG_1 - FBG_2$ power difference are − 0.07 nm/℃ and 0.35 dB/℃, respectively, which indicates that the differential detection sensing system has cross-sensitivity.

3.3. Fabrication of biological probe

In the experiment, Tris-Hydrochloride is used to dissolve DA. Mix and shake 1 mL of hydrochloric acid buffer and 2 mg of DA to configure a 2 mg/mL solution. The MFI is immersed in this PDA solution for some time and removed from the this solution at about 8 nm wavelength drift During this process, DA gradually polymerizes, reflecting the gradual change from colorless to black, and a uniform PDA film is formed on the microfiber surface. In Fig. 5 (a) the transmission spectrum is redshifted with the increase of time. Fig. 5 (b) shows the change in the wavelength shift of the MFI and the power difference of grating during the plating of the PDA film. The sensitivity of the MFI is 0.22 nm/min, and the sensitivity of $FBG_1 - FBG_2$ is 0.44 dB/min.

Then, configure a 30 mM mixture of β-CD: propofol mixed solution. Firstly, 0.8 g of β-CD is added to 10 mL of DI water and stirred at 60℃ for 15 min to obtain β-CD solution. After this, mix 1 mL of propofol, 1 mL of β-CD solution and 89 ml of DI water, and ultrasonic stirring is performed for 3 h to obtain 30 mM of β-CD: propofol (v: v 1: 1) mixed solution. The propofol functional film is obtained by dropping β-CD: propofol solution on the coated PDA microfiber for remaining for 20 min. Fig. 5 (c) shows the change in the wavelength shift of the MFI and the power difference of grating during the plating of propofol functional film. The sensitivity of the MFI is 0.01 nm/min, and the sensitivity of $FBG_1 - FBG_2$ 0.03 dB/min.

Finally, configure the template to remove the solution. 1 mL of Triton x–100 is added to 10 mL of DI water, stirred at room temperature (26℃)

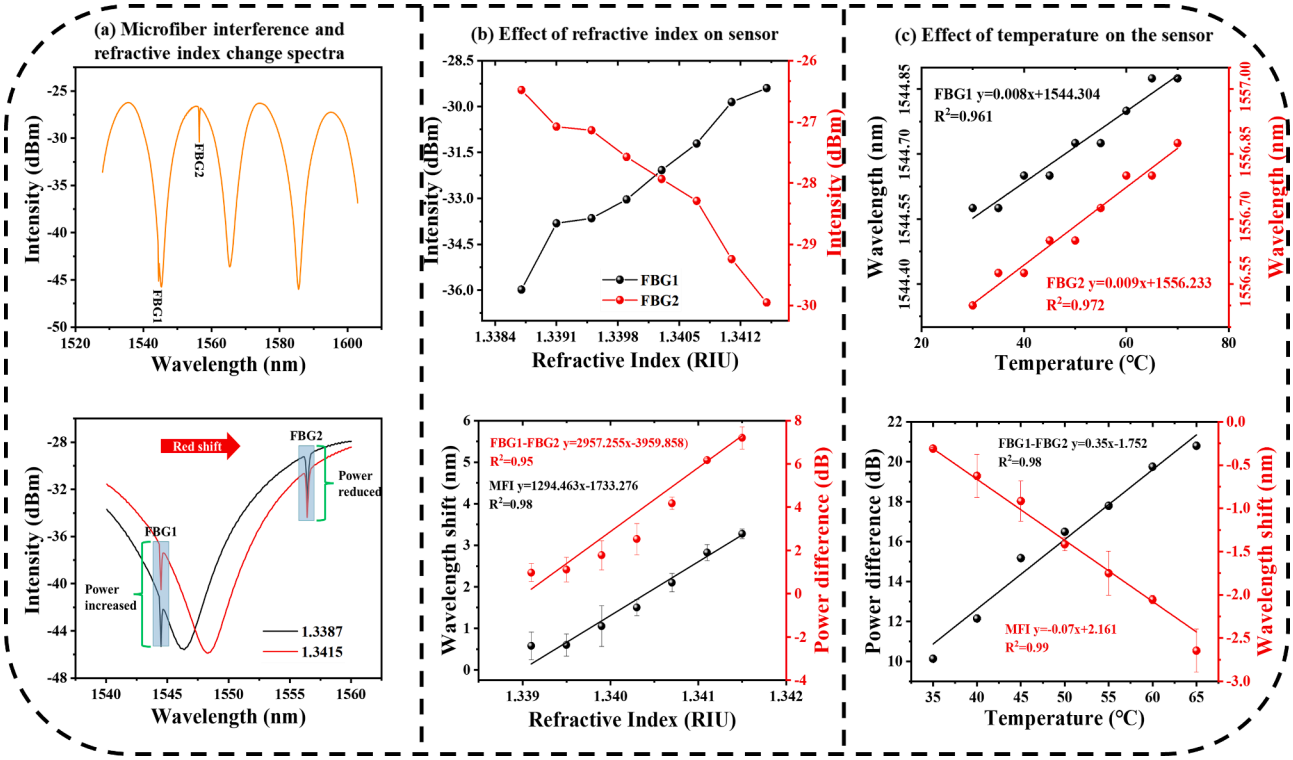

Fig. 4. The initial spectra of sensors (Top) and the transmission spectra of refractive index variations (Bottom); (b) Power varition of two FBGs (Top) and RI response of the FBG power difference and the interference wavelength (Bottom); (c) Temperature response of two FBG wavelength (Top) and temperature response of the FBG power difference and the interference wavelength (Bottom).

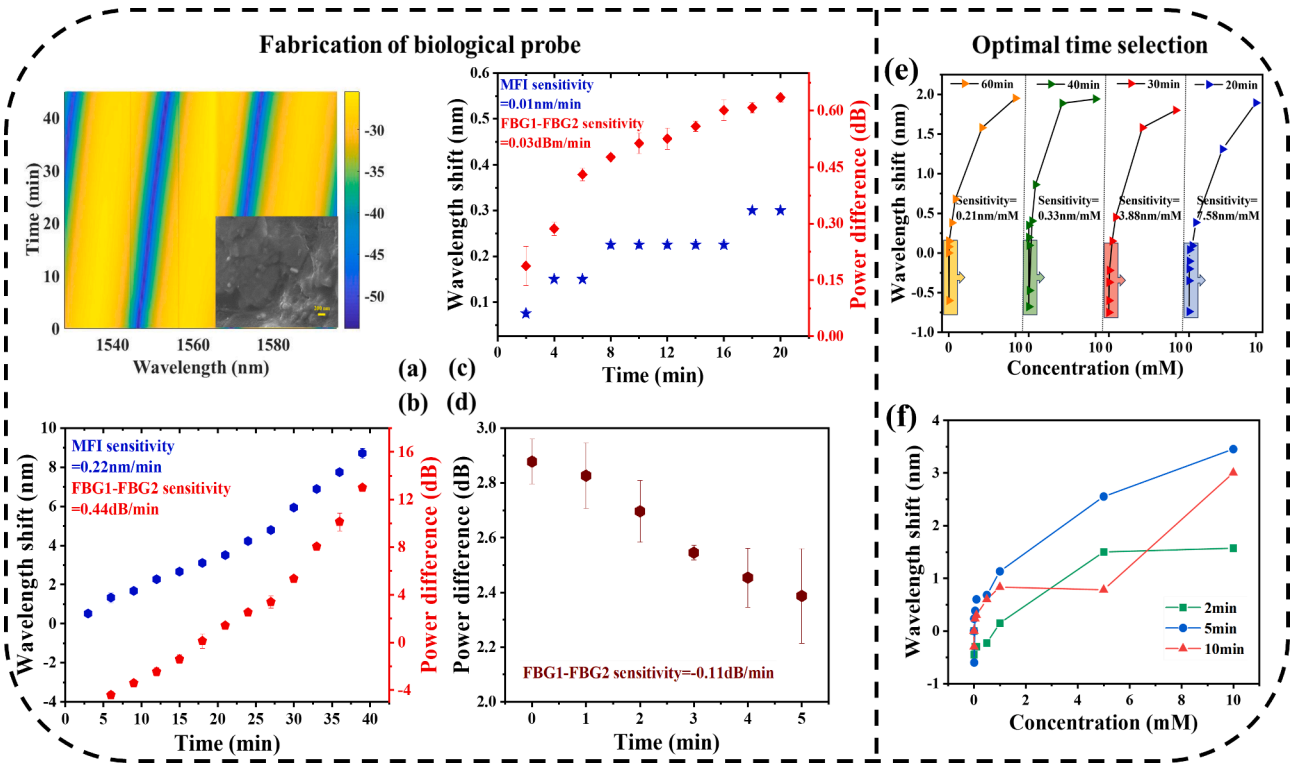

Fig. 5. (a) Changing of wavelength drift spectra; (b) Effecting of PDA film plating on microfiber and grating spectra; (c) MFI coating β-CD:propofol mixed solutions changes in interference wavelength and grating power; (d) The influence of template removal process on the wavelength shift of MFI; (e) The selection of the best coating β-CD: propofol mixed solutions time; (f) The selection of the best template removal time.

for 10 min for obtaining a mixed solution, which is applied to the surface of the MFI for propofol functional film. After standing for 5 min, the propofol on functional membrane is washed to obtain MIP sensor with specific recognition of propofol. Fig. 5 (d) shows the response of FBGs power difference during template removal.

In the experimental stage, in order to select the best coating time of β-CD: propofol mixed film on microfiber surface, 20 min, 30 min, 40 min and 60 min are selected in order to optimize the performance of the sensors with other preparation conditions remaining constant (template removal time of 5 min). These prepare MIP sensors are used to investigate the detection ability of propofol in the concentration range of 0.001 mM–10 mM. As shown in Fig. 5 (e), the first five points are selected at propofol concentrations of 0.001–10 mM and their wavelength drift sensitivities are calculated, which are 0.21 nm/mM for 60 min, 0.33 nm/mM for 40 min, 3.88 nm/mM for 30 min, and 7.58 nm/mM for 20 min, respectively. And the corresponding wavelength drifts are 1.95 nm, 2.55 nm, 2.55 nm and 3.45 nm, respectively. It can be concluded that 20 min is the optimum coating time. The reason for this phenomenon is that if the immersion time in the β-CD: propofol mixed solution is too short, too little polymer may be attached to the PDA layer, resulting in insufficient specific binding sites. When the immersion time of the polymeric solution is too long, it may cause the polymer layer on the microfiber surface to be too thick, which is not conducive to the increase of RI sensitivity and leads to larger spectral losses. It should be noted that there is a trade-off between RI sensitivity and transmission loss (as well as stability) [28,29]. In summary, the time of 20 min for coating β-CD: propofol films is chosen.

The detecting ability of propofol biodetection probes is obtained by comparing different template removal times. Selecting the most recent template removal time, as shown in Fig. 5 (f). Under the precondition that other preparation conditions remain unchanged (β-CD: propofol mixed film coating time of 20 min), template removal times of 2 min, 5 min and 10 min are selected. These prepared MIP sensors can detect propofol concentration of 0.001–10 mM. Fig. 5 (f) shows that the wavelength shift of 10 min is 1.57 nm, that of 5 min is 3.45 nm, and that of 2 min is 3 nm, which is concluded that 5 min is the better time. The reason for this phenomenon is that when the template removal time is too short, the template molecules in the polymer may not be completely removed, resulting in insufficient specific binding sites. However, when the template removal time is too long, it may cause part of the PDA layer on the microfiber surface to be washed away, so 5 min is the best template removal time.

3.4. Detection of propofol

By placing the MIP sensor in DI water before the start of the detection experiment, it can be seen that the sensor can exclude the influence of DI water, as shown in Fig. 6 (a). The perturbed MFI wavelength drift is 0.073 nm, and the perturbed FBGs power change is 0.009 dB.

In the test, these propofol solutions of 0.001, 0.005, 0.01, 0.05, 0.1, 0.5, 1, 5 and 10 (in mM) concentrations are prepared. Specifically, first dissolve 1 mL of propofol in 1 mL of Triton x–100 solution and stir at room temperature for 20 min to obtain a mixed solution of propofol. Then take 1 mL propofol mixed solution and add 269 mL DI water to get 10 mM propofol aqueous solution. The optical fiber MIP sensor starts from the minimum concentration and detects each concentration for 3 min. The spectrum at the final stabilization is selected as the most important data in this study.

The transmission spectra at different concentrations of propofol are shown in Fig. 6 (b). As can be seen from the figure, the redshift on the wavelength occurs as the concentration increases. Fig. 6(c) shows the error bar analysis of the repeated experiments of concentration detection, and the change of the power difference between the MFI and the FBGs. The relationship between the concentration at 0.001 to 10 mM and wavelength shift and FBGs power difference, and the fitting of the infrount four points is shown in the illustration in Fig. 6 (c). the fitting wavelength shift sensitivity is 6.04 nm/mM, and the FBGs power difference sensitivity is 10.89 dB/mM. Fig. 6 (d) shows that the linear

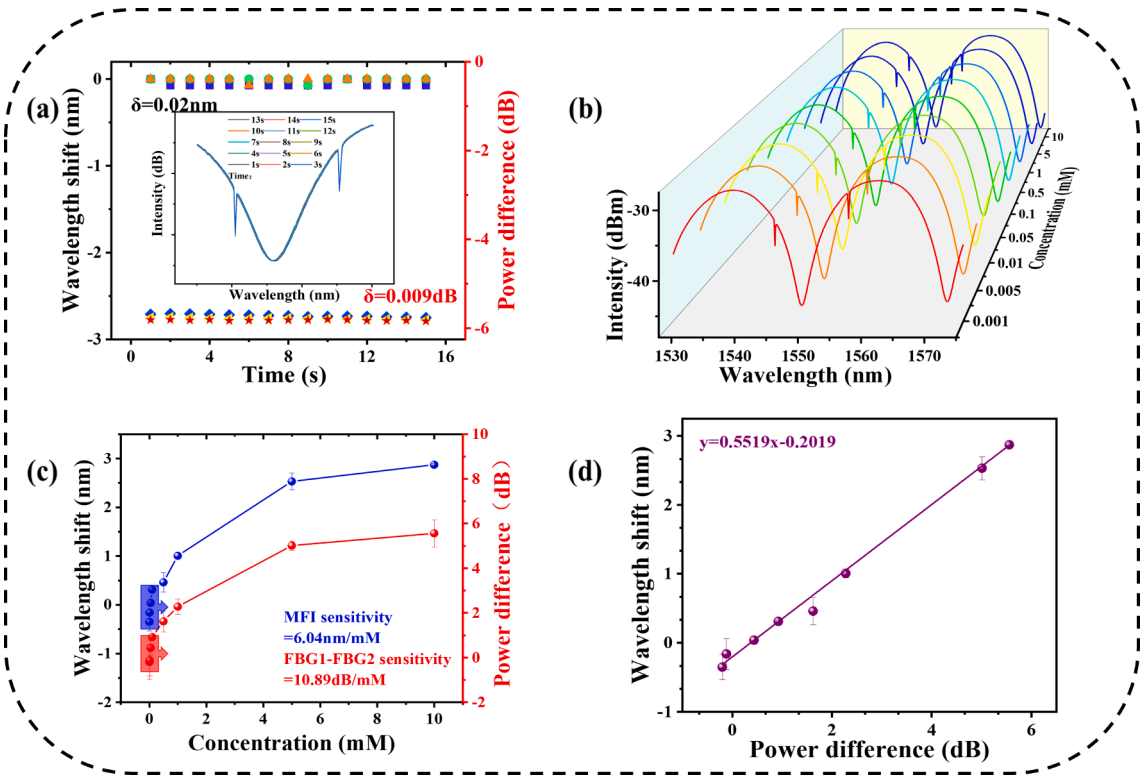

Fig. 6. (a) MIP sensor system stability measurement; (b) Wavelength shift diagram for concentration detection; (c) The variation of MFI and FBGs power difference error bar with concentration; (d) Linear relationship between power difference and wavelength shift.

relationship between power difference and wavelength shift can be represented by $y = 0.5519x - 0.2019$. Therefore, the wavelength shift can be calculated by obtaining the power difference of FBGs, which indicates that OPM can replace the spectral analyzer to monitor the optical response of the sensing system.

3.5. Specific detection

The specific response of the sensor to the measured substance is an important index to indicate the performance of the sensor. In order to verify the sensor's specific recognition, eight kinds of substances with similar structure and molecular weight to propofol, except DI water, are selected to perform specific experiments on the MIP sensor within the concentration range of 0.001 to 10 mM, and the experiments are repeated some times for each substance to exclude the influence of chance on the experimental results. In Fig. 7, the experimental results show that the redshifts of the highest concentrations of DI water, paracetaminophenol, glucose, uric acid, cholesterol, thymol and eugenol are 0 nm, 0.833 nm, 0.503 nm, 0.59 nm, 0.345 nm, 1.12 nm and 0.565 nm, respectively and some substances have blue shift in other concentrations. Thus, these results indicate that the response of the MIP sensor to propofol is much higher than that of other substances, and the sensor has

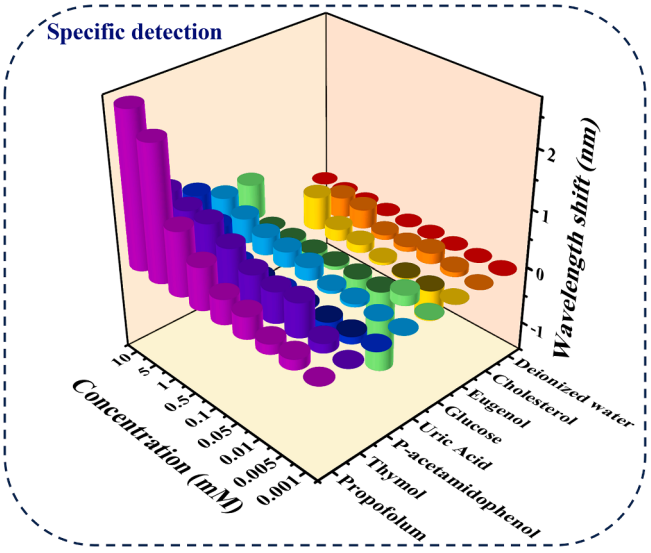

Fig. 7. The specific detection of the MIP sensor to propofol and specific substances (DI water, paracetamol, glucose, uric acid, cholesterol, thymol and eugenol) within the concentration range of 0.001–10 mM.

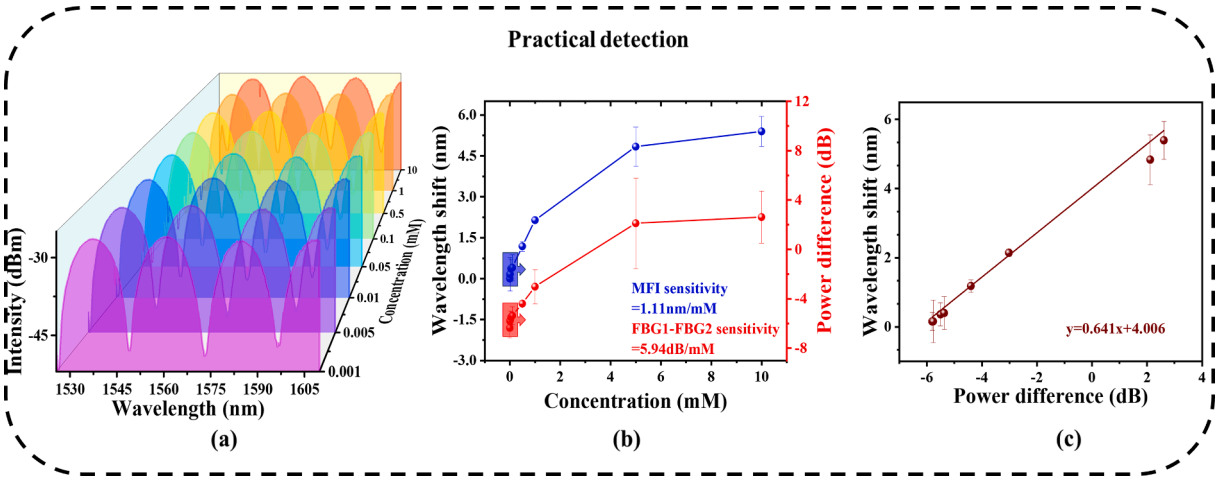

Fig. 8. (a) Wavelength shift diagram for concentration detection in artificial urine environment; (b) The variation of microfiber interferometer and grating power difference error bar with concentration; (c) Linear relationship between power difference and wavelength shift.

a good specific recognition of propofol.

3.6. Practical detection

In order to verify that the all fiber sensing system has good sensing performance in the actual application, the artificial urine is utilized to simulate the actual environment to detect propofol. Artificial urine is used because actual urine contains a lot of impurities (the cations Na, K, NH_4, Ca and the anions, C1, SO_4, PO_4 and HCO_3, escherichia, coli Aerobacter aerogenes, pseudomonas aeruginosa, proteus mirabilis, enterococcus, staphylococcus aureus and staphylococcus albus Etc.) [30].

In the test, these propofol solutions of 0.001, 0.005, 0.01, 0.05, 0.1, 0.5, 1, 5, and 10 (in mM) concentrations adding in artificial urine are prepared. As shown in Fig. 8. it is the response of the sensor to propofol in the artificial urine environment. The sensor starts from the minimum concentration and detects each concentration for 3 min (Consistent with

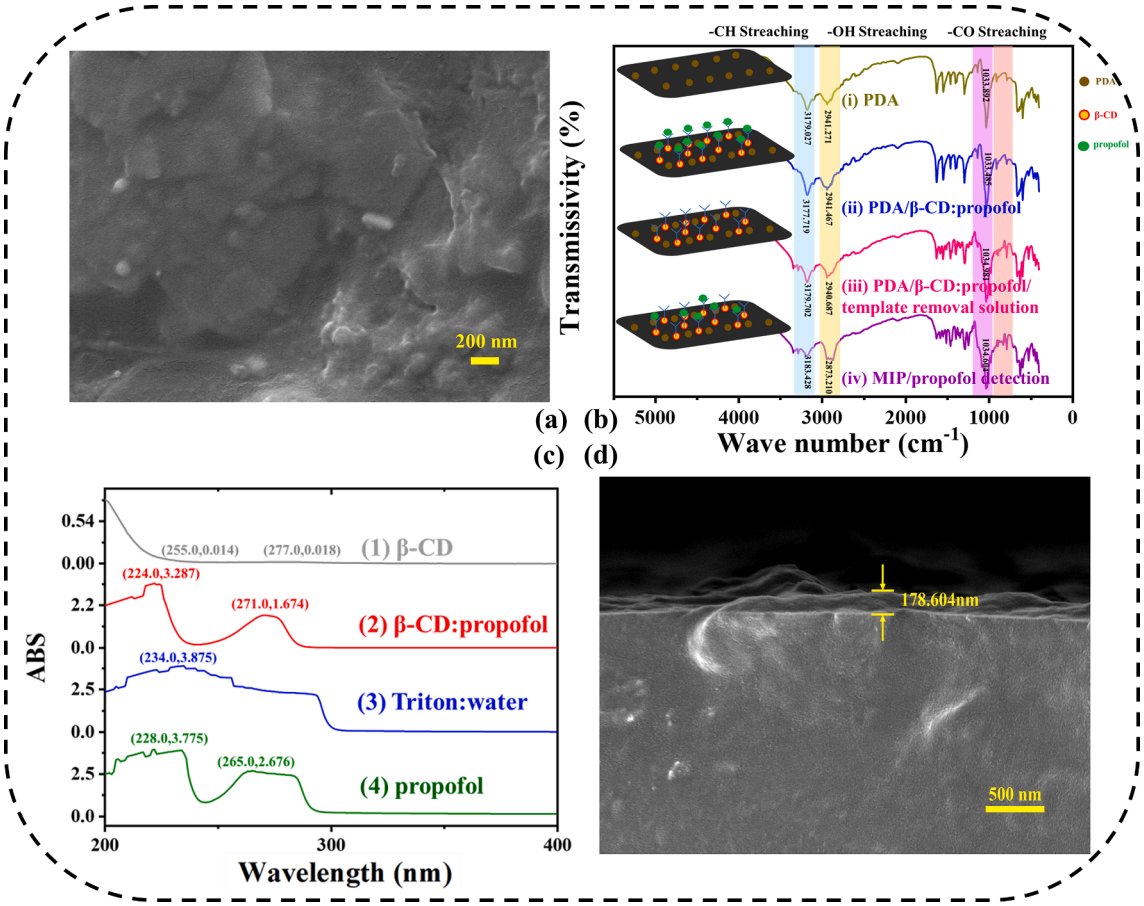

Fig. 9. (a) SEM image with 30,000x PDA magnification; (b) PDA, PDA/β-CD: propofol, PDA/β-CD: propofol/template removal solution and MIP/propofol detection ATR-FTIR spectrometer analysis; (c) UV-vis spectra of (1) β-CD; (2) β-CD: propofol; (3) Triton: water; (4) propofol; (d) SEM image with 20,000× MIP films magnification.

the sensor detecting propofol in DI water). The spectrum at the final stability is selected as the most important data in this study. Fig. 8.(a) shows that the spectrum of the sensor shifts to the right as the concentration of propofol increases. It can be seen from the figure that the redshift on the wavelength of MFI occurs with the increase of the concentration, while the light intensity of FBG_1 increases and that of FBG_2 decreases. Fig. 8 (b) shows the error bar analysis of the repeated experiments of concentration detection, and the change of the power difference between the MFI and the grating. For the relationship between the concentration of 0.001 to 10 mM and wavelength drift and FBGs power difference, the fitting of the infrount four points is shown in the illustration in Fig. 8 (b). The fitting sensitivity of wavelength drift is 1.11 nm/mM, and the grating power difference sensitivity is 5.94 dB/mM. Fig. 8 (c) shows that the linear relationship between power difference and wavelength drift can be represented by $y = 0.641x + 4.006$. Therefore, the wavelength shift can be calculated by obtaining the power difference of FBGs.

3.7. Sensor characterization

In order to elucidate the interaction between the components of the sensor film, the characteristics of the optical fiber coated with PDA film is performed to observe by SEM. Fig. 9 (a) is the SEM image of the PDA film on the surface of the optical fiber. When the optical fiber is immersed in PDA solution for 40 min, it can be seen that the surface of the optical fiber is covered by uniform particles [31,32].

The composition of MIP films is determined by attenuated total reflection Fourier transform infrared (ATR-FTIR) spectrometer. The National Institute of Standards and Technology (NIST) in the United States reported the wave numbers of the strongest vibration modes of propofol measured by FTIR, which ar: 3610 cm^{-1}, 2930–2850 cm^{-1}, 1410 cm^{-1} and 1170 cm^{-1}. Four samples on the coated slides of (i) PDA、(ii) PDA/ β-CD: propofol、(iii) PDA/ β-CD: propofol/template removal solution and (iv) MIP/propofol detection are performed by ATR-FTIR spectrometer analysis. Sample (iii) is added with Triton x–100: DI water (v: v 1: 10) as a template removal solution to wash off propofol on the surface of the film. The characterization results are shown in Fig. 9(b). The wide peak of the PDA at 3200–2900 cm^{-1} is due to the O–H and N–H stretching vibration peaks [33]. The absorption peak at 2941 cm^{-1} in sample (ii) is the characteristic absorption of β-CD: propofol, which is indicated by the changes in O–H vibration here binding of β-CD: propofol inclusion complex with PDA [34].The absorption peaks at 3177–3184 cm^{-1} and 1033–1035 cm^{-1} are respectively the stretching vibration of C–H and the stretching vibration of C–O [31]. Comparing sample (iii) and sample (iv) at 787 cm^{-1}–910 cm^{-1}, it can be seen that sample (iii) has no peak value, but sample (iv) does, indicating that sample (iii) has no propofol and sample (iv) has the presence of propofol [35].

The binding of propofol to β-CD and the binding of propofol to Triton x–100 are identified by Ultraviolet-visible spectroscopy (UV-vis). It is a common method for forming cyclodextrin inclusions with guest molecules [36,37]. Sample (1) in Fig. 9 (c) is the UV-vis spectrum of β-CD [38]. It can be seen from (b) that β-CD does not show any absorption spectrum in the entire wavelength range. In aqueous solution, there are two strong maximum absorption peaks at 224 nm and 271 nm. The UV-vis of sample (2) shows a slight broadening of the maximum absorption peak from 200 to 300 nm, confirming the formation of the β-CD: propofol inclusion complex. The decrease in absorbance indicates that propofol is encapsulated in a hydrophobic β-CD cavity [8]. Because propofol is insoluble in DI water, Triton x–100 is used as the co solvent for propofol in this design.The combination of propofol and Triton is identified by UV-vis spectroscopy, as shown in Fig. 9 (c). In Fig. 9 (c), sample (3) is the UV-vis spectrum of Triton x–100, with an absorption spectrum at 234 nm [9]. sample(4) is the spectrum of the mixed aqueous solution of propofol and Triton x–100, with two strong maximum absorption peaks at 228 nm and 265 nm. The UV absorption mode of the mixed aqueous solution showed a slight broadening of the maximum absorption peak from 200 to 300 nm, which confirmed that propofol is dissolved by Triton x–100. The decrease in absorbance indicates that propofol is encapsulated in a hydrophobic triton cavity [10].

In order to visually characterize the MIP films, we prepare the characterized sample, which is a functional film mentioned in the manuscript, is coated on an ordinary single-mode optical fiber. The instrument used in the process of characterization is scanning electron microscopy (SEM, Zeiss Sigma 300, Germany). As shown in Fig. 9 (d), the thickness of the functional film on the optical fiber surface is about 178.604 nm.

Table 1 shows a comparison of this work with some of the popular methods currently used to detect isoproterenol concentrations. Optical methods used in [1,7] have significant advantages for improving the specificity of the propofol sensor, but the disadvantages such as the high cost of preparation and the requirement of high signal processing equipment should not be ignored. The use of electrochemical detection techniques [5,6,39,40] have the advantages of accuracy and sensitivity, but the insoluble polymers produced by the electrochemical reaction passivate the surface of the electrodes to reduce the detection accuracy and lifetime. In contrast, the paper proposed sensing system is not only simple to fabricate and less costly, but also can more accurately detect isoproterenol concentration in the low concentration range by detecting the interferometric wavelength drift and FBG power difference.

Table 1
The different structures of the sensor to detect propofol.

Structure and material	Connector identification element	Concentration range	Sensor sensitivity	LOD	Publication date	Reference
Handheld analyzer and disposable plastic lab on a chip	MIP label-free electrical detection techniques	$6 \times 10^{-4}$to 0.18 mM	–	6×10^{-4}mM	2016	[1]
Electrochemical cleaning procedure for long-term electrochemical monitoring	Boron-doped diamond (BDD) and pencil graphite electrode (PGE)	$9.9 \times 10^{-3}$to 8.05 $\times 10^{-2}$mM	1.1×10^{-2}μA/μM	$(0.82 \pm 0.08) 10^{-3}$mM	2018	[39]
An enzyme-based electrochemical biosensor	Cytochrome P450 2B6,gold nanoparticles and chitosan film	6×10^{-3} to 6×10^{-2}mM	4.2 ± 0.2nA/μg/ml/mm^2	4.02×10^{-5}mM	2021	[5]
U-shape functionalized optical fiber sensor	MIP liquid-phase deposition propofol techniques	1×10^{-3} to 8×10^{-3} mM	–	6.9×10^{-4}mM	2022	[7]
An electrochemical microcatheter sensor	$Ti_3C_2T_x$-rGO-chitosan-based microcatheter	5×10^{-3} to 0.11 mM	–	2×10^{-3}mM	2023	[6]
A disposable electrochemical sensor	Composite of SnO_2 nanoparticle and Nb_2CTx MXene (SnO_2/Nb_2CTx)	1×10^{-3} to 0.3 mM	0.26 μA/μM/cm^2	2.4×10^{-4}mM	2024	[40]
Functional micro fiber interferometer and two-stage fiber Bragg gratings	Molecularly imprinted films bound to polydopamine	1×10^{-3} to 10 mM	6.04 nm/mM 10.89 dB/mM	2×10^{-3}mM	2024	This work

4. Conclusion

This paper present a differential sensing system based on the combination of MFI coated with MIP films and FBGs for for the measurement of propofol. The MIP combination of target molecule causes the surface RI change, which is converted into the interference wavelength shift for resulting in a change in the FBGs power difference. The experimental results of detecting propofol concentration in DI water show that the sensor has obvious response in the concentration range of 0.001–10 mM, and the sensitivity is as high as 6.04 nm/mM and 10.89 dB/mM. For further research, the system also has excellent sensing performance in artificial urine environment, the sensitivity of MFI is 1.11 nm/mM and the two FBGs power difference sensitivity is 5.94 dB/mM. The ATR-FTIR spectrometer shows that the sensor can indeed detect propofol. This differential sensing system has a few strong advantages of high sensitivity and good selectivity, which expects great potential in biomedical applications.

CRediT authorship contribution statement

Bowen Yang: Writing – original draft, Investigation, Formal analysis, Data curation. **Li Jin:** Investigation, Data curation. **Ze Xu:** Investigation, Data curation. **Wenwen Wang:** Methodology, Data curation. **Guanjun Wang:** Project administration, Funding acquisition. **Jizhou Wu:** Project administration, Funding acquisition. **Dandan Sun:** Writing – review & editing, Methodology, Investigation, Funding acquisition. **Jie Ma:** Resources, Project administration, Funding acquisition.

Declaration of competing interest

The authors declare that they have no known competing financial interests or personal relationships that could have appeared to influence the work reported in this paper.

Data availability

Data will be made available on request.

Acknowledgments

This work was supported by National Natural Science Foundation of China (62005147, 62175054, 62175140, U2341211, 62020106014).

Appendix A. Supplementary data

Supplementary data to this article can be found online at https://doi.org/10.1016/j.microc.2024.111121.

References

[1] C. Hong, C. Lin, C. Hong, Z. Lin, M. Chung, P. Hsieh, Handheld analyzer with on-chip molecularly-imprinted biosensors for electrical detection of propofol in plasma samples, Biosens. Bioelectron. 86 (2016) 623–629, https://doi.org/10.1016/j.bios.2016.07.032.

[2] T. Zhong, Y. Lin, R. Zhuge, Y. Lin, B. Huang, R. Zeng, Reviewing the mechanism of propofol addiction, All Life 16 (1) (2023) 2174708, https://doi.org/10.1080/26895293.2023.2174708.

[3] F. Maurer, T. Shopova, B. Wolf, D. Kiefer, T. Hüppe, T. Volk, D. Sessler, S. Kreuer, Design and validation of an automated solid phase extraction liquid chromatography coupled mass spectrometry method for the quantification of propofol in plasma, J. Pharm. Biomed. Anal. 150 (2018) 341–346, https://doi.org/10.1016/j.jpba.2017.12.043.

[4] F. Maurer, M. Geiger, T. Volk, D. Sessler, S. Kreuer, Validation of liquid and gaseous calibration techniques for quantification of propofol in breath with sorbent tube Thermal Desorption System GC-MS, J. Pharm. Biomed. Anal. 143 (2017) 116–122, https://doi.org/10.1016/j.jpba.2017.05.042.

[5] D. Ferrier, J. Kiely, R. Luxton, Cytochrome P450 2B6 amperometric biosensor for continuous monitoring of propofol, IEEE Sens. J. 21 (21) (2021) 23730–23736, https://doi.org/10.1109/JSEN.2021.3112273.

[6] C. Kafley, R.K.S. Kummari, K. Lakavath, Y. Kotagiri, Ti_3C_2T x–rGO-chitosan-based microcatheter sensor for real-time continuous monitoring of propofol: toward improved anesthetic management, Microchim. Acta 190 (10) (2023) 388, https://doi.org/10.1007/s00604-023-05969-8.

[7] F. Hernandez, T. Wang, S. Lee, A. Norris, L. Liu, B. Hayes-Gill, S. Morgan, S. Korposh, U-shape functionalized optical fibre sensors for measurement of anaesthetic propofol, Sensor Actuat. B-Chem. 372 (2022) 132653, https://doi.org/10.1016/j.snb.2022.132653.

[8] A. Shrivastav, S. Mishra, B. Gupta, Fiber optic SPR sensor for the detection of melamine using molecular imprinting, Sensor Actuat. B-Chem. 212 (2015) 404–410, https://doi.org/10.1016/j.snb.2015.02.028.

[9] H. Agrawal, A. Shrivastav, B. Gupta, Surface plasmon resonance based optical fiber sensor for atrazine detection using molecular imprinting technique, Sensor Actuat. B-Chem. 227 (2016) 204–211, https://doi.org/10.1016/j.snb.2015.12.047.

[10] P. Gorai, Y. Mizuno, M. Kumar, R. Jha, Molecular imprinting polymer nanoparticles coupled with an optical sensor for sensitive and label-free detection of p-cresol, ACS Appl. Nano Mater. 6 (14) (2023) 12946–12956, https://doi.org/10.1021/acsanm.3c01681.

[11] L. Sun, J. Li, Y. Tan, S. Gao, L. Jin, B. Guan, Bending effect on modal interference in a fiber taper and sensitivity enhancement for refractive index measurement, Opt. Express 21 (2013) 26714–26720, https://doi.org/10.1364/OE.21.026714.

[12] D. Sun, Y. Hao, Y. Fu, J. Ma, Organic dye concentration monitoring through anoptical microfiber enabled by multiwalled carbon nanotubes, J. Opt. Soc. Am. B 38 (2021) 178–185, https://doi.org/10.1364/JOSAB.433550.

[13] D. Sun, Y. Ran, G. Wang, Label-free detection of cancer biomarkers using an in-line taper fiber-optic interferometer and a fiber bragg grating, Sensors 17 (2017) 2559, https://doi.org/10.3390/s17112559.

[14] J. Fleming, Dispersion in GeO_2–SiO_2 glasses, Appl. Opt. 23 (1984) 4486, https://doi.org/10.1364/AO.23.004486.

[15] R. Parc, B. Champagnon, C. Levelut, V. Martinez, L. David, A. Faivre, I. Flammer, J. Hazemann, J. Simon, Density and concentration fluctuations in SiO_2–GeO_2 optical fiber glass investigated by small angle x-ray scattering, J. Appl. Phys. 103 (2008) 094917, https://doi.org/10.1063/1.2917384.

[16] Y. Tan, T. Huang, L. Sun, S. Jiang, Y. Liu, B. Guan, W. Jin, Dispersion turning point-enhanced photothermal interferometry gas sensor with an optical microfiber interferometer, Sensor Actuat. B-Chem. 385 (2023) 133690, https://doi.org/10.1016/j.snb.2023.133690.

[17] V. Bhardwaj, K. Kishor, A. Sharma, Tapered optical fiber geometries and sensing applications based on Mach-Zehnder Interferometer: A review, Opt. Fiber Technol. 58 (2020) 102302, https://doi.org/10.1016/j.yofte.2020.102302.

[18] X. Zhu, C. Jiang, X. Guo, H. Chen, S. Sun, C. Liu, High-sensitivity temperature sensor based on Mach-Zehnder interferometer filled with dimethyl silicone oil, Meas. Sci. Technol. 34 (1) (2022) 015111, https://doi.org/10.1088/1361-6501/ac8f64.

[19] Y. Huang, Z. Tian, L. Sun, D. Sun, J. Li, Y. Ran, B. Guan, High-sensitivity DNA biosensor based on optical fiber taper interferometer coated with conjugated polymer tentacle, Opt. Express 23 (21) (2015) 26962–26968, https://doi.org/10.1364/oe.23.026962.

[20] D. Sun, Y. Fu, Y. Yang, Label-free detection of breast cancer biomarker using silica microfiber interferometry, Opt. Commun. 463 (2020) 125375, https://doi.org/10.1016/j.optcom.2020.125375.

[21] C. Tavares, C. Leitão, D. Presti, M. Domingues, N. Alberto, H. Silva, P. Antunes, Respiratory and heart rate monitoring using an FBG 3D-printed wearable system, Biomed. Opt. Express 13 (4) (2022) 2299–2311, https://doi.org/10.1364/BOE.452115.

[22] L. Soldano, E. Pennings, Optical multi-mode interference devices based on self-imaging: principles and applications, J. Lightwave Technol. 13 (4) (1995) 615–627, https://doi.org/10.1109/50.372474.

[23] Z. Niu, I. Thielen, A. Barnett, S. Loveday, H. Singh, ε-Polylysine and β-cyclodextrin assembling as delivery systems for gastric protection of proteins and possibility to enhance intestinal permeation, J. Colloid Interface Sci. 546 (2019) 312–323, https://doi.org/10.1016/j.jcis.2019.03.006.

[24] F. Maestrelli, M. Bragagni, P. Mura, Advanced formulations for improving therapies with anti-inflammatory or anaesthetic drugs: A review, J. Drug Deliv. Sci. Tec. 32 (2016) 192–205, https://doi.org/10.1016/j.jddst.2015.09.011.

[25] S. Hong, Y. Na, S. Choi, I. Song, W. Kim, H. Lee, Non-covalent self-assembly and covalent polymerization co-contribute to polydopamine formation, Adv. Funct. Mater. 22 (22) (2012) 4711–4717, https://doi.org/10.1002/adfm.201201156.

[26] E. Faure, C. Falentin-Daudré, C. Jérôme, J. Lyskawa, D. Fournier, P. Woisel, C. Detrembleur, Catechols as versatile platforms in polymer chemistry, Prog. Polym. Sci. 38 (1) (2013) 236–270, https://doi.org/10.1016/j.progpolymsci.2012.06.004.

[27] S. Yap, Y. Chien, R. Tan, A. Alauddin, W. Ji, S. Tjin, K. Yong, An advanced hand-held microfiber-based sensor for ultrasensitive lead ion detection, ACS Sens. 3 (12) (2018) 2506–2512, https://doi.org/10.1021/acssensors.8b01031.

[28] L. Sun, T. Huang, Z. Yuan, W. Lin, P. Xiao, M. Yang, J. Ma, Y. Ran, L. Jin, J. Li, B. Guan, Ultra-high sensitivity of dual dispersion turning point taper-based Mach-Zehnder interferometer, Opt. Express 27 (2019) 23103–23111, https://doi.org/10.1364/OE.27.023103.

[29] G. Wang, D. Sun, L. Liang, G. Wang, J. Ma, Highly sensitive detection of trace lead ions concentration based on a functional film-enhanced optical microfiber sensor, Opt. Laser Technol. 161 (2023) 109171, https://doi.org/10.1016/j.optlastec.2023.109171.

[30] J. Yao, T. Wu, Y. Sun, Z. Ma, M. Liu, Y. Zhang, S. Yao, A novel biomimetic nanoenzyme based on ferrocene derivative polymer NPs coated with polydopamine, Talanta 195 (2019) 265–271, https://doi.org/10.1016/j.talanta.2018.11.069.

[31] J. Jiang, L. Zhu, L. Zhu, B. Zhu, Y. Xu, Surface characteristics of a self-polymerized dopamine coating deposited on hydrophobic polymer films, Langmuir 27 (23) (2011) 14180–14187, https://doi.org/10.1021/la202877k.
[32] D. Kaye, Antibacterial activity of human urine, J. Clin. Invest. 47 (10) (1968) 2374–2390, https://doi.org/10.1172/JCI105921.
[33] C. Jimmy, Z. Jiang, H. Liu, J. Yu, L. Zhang, β-Cyclodextrin epichlorohydrin copolymer as a solid-phase extraction adsorbent for aromatic compounds in water samples, Anal. Chim. Acta 477 (1) (2003) 93–101, https://doi.org/10.1016/S0003-2670(02)01411-3.
[34] S. Prabu, K. Sivakumar, S. Nayaki, R. Rajamohan, Host-guest interaction of cytidine in β-cyclodextrin microcavity: Characterization and docking study, J. Mol. Liq. 219 (2016) 967–974, https://doi.org/10.1016/j.molliq.2016.04.017.
[35] A. Abou-Okeil, M. Rehan, S. El-Sawy, M. El-bisi, O. Ahmed-Farid, F. Abdel-Mohdy, Lidocaine/β-cyclodextrin inclusion complex as drug delivery system, Eur. Polym. J. 108 (2018) 304–310, https://doi.org/10.1016/j.eurpolymj.2018.09.016.
[36] A. Trapani, V. Laquintana, A. Lopedota, M. Franco, A. Latrofa, G. Talani, E. Sanna, G. Trapani, G. Liso, Evaluation of new propofol aqueous solutions for intravenous anesthesia, Int. J. Pharm. 278 (1) (2004) 91–98, https://doi.org/10.1016/j.ijpharm.2004.02.028.
[37] E. Nasybulin, S. Wei, I. Kymissis, K. Levon, Effect of solubilizing agent on properties of poly (3, 4–ethylenedioxythiophene) (PEDOT) electrodeposited from aqueous solution, Electrochim. Acta 78 (2012) 638–643, https://doi.org/10.1016/j.electacta.2012.06.083.
[38] Y. Espinosa, E. Caffarena, Y. Martínez, J. Grigera, Pressure effect on micellization of non-ionic surfactant Triton X–100, J. Chem. Phys. 148 (7) (2018) 074901, https://doi.org/10.1063/1.5003358.
[39] F. Stradolini, T. Kilic, I. Taurino, G. De Micheli, S. Carrara, Cleaning strategy for carbon-based electrodes: Long-term propofol monitoring in human serum, Sensor Actuat. B-Chem. 269 (2018) 304–313, https://doi.org/10.1016/j.snb.2018.04.082.
[40] M. Ankitha, P. Vaishag, P. Muhsin, P. Rasheed, Flexible and disposable electrodes based on SnO_2 nanoparticle/Nb_2CTx nanosheet composites for selective and ultrasensitive detection of propofol, J. Ind. Eng. Chem. 131 (2024) 449–458, https://doi.org/10.1016/j.jiec.2023.10.049.